Publ. Astron. Soc. Aust., 1998, 15, 70–3

CO Observations of the λ-Orionis Ring

W. J. Lang[1] and M. R. W. Masheder[1]

[1]H. H. Wills Physics Laboratory, Bristol University, Tyndall Ave, Bristol, BS8 1TL, UK
w.j.lang@bristol.ac.uk, mike.masheder@bristol.ac.uk

Received 1997 August 1, accepted 1997 December 11

Abstract: We present results from a new ^{12}CO ($J = 1 \rightarrow 0$) survey of the λ-Orionis region. The observations cover 110 square degrees uniformly on a Nyquist-sampled grid. We discover CO emission at levels far lower than possible in previous surveys, revealing a structure similar to that seen in IRAS 100μ maps. We derive a total molecular mass of $1{\cdot}1{\times}10^4$ $M_\odot$. A possible explanation for the isolated and localised outbreak of star formation in the region is discussed.

Keywords: ISM: bubbles — ISM: clouds — ISM: HII regions — ISM: molecules

1 Observations

Using the $1{\cdot}2$ m radio telescope at the Harvard–Smithsonian Center for Astrophysics, we have surveyed a $10^\circ{\times}11^\circ$ area covering the λ-Orionis OB association (Murdin & Penston 1977), the HII region S264 (e.g. Reich 1978) and the prominent surrounding ring of dust (Zhang et al. 1989) and gas (Wade 1957; Maddalena & Morris 1987 — henceforth 'MM'). The data were taken on a uniform grid in Galactic Coordinates with half-beamwidth sampling. The telescope HPBW is $8{\cdot}4'$ at 115 GHz, corresponding to $1{\cdot}16$ pc at 400 pc, the estimated distance to the λ-Ori association. The 28,855 spectra each have a sensitivity per channel of $0{\cdot}25$ K ($T_{\rm mb}$), and velocity resolution is $0{\cdot}65$ km s^{-1}. The resulting datacube (v, l, b) is smoothed to $10'$ resolution at $0{\cdot}12$ K sensitivity, covering the velocity range $[-10, +20]$ km s^{-1} with respect to the LSR.

2 Results

To obtain maximum signal-to-noise in two-dimensional maps from the datacube we use the masked moment analysis technique (e.g. Digel et al. 1996). Figure 1 displays a zeroth moment $W_{\rm CO}$ map. The equivalent of the lowest contour in the MM map lies at the ≈3 K km s^{-1} level in the new map. The much greater depth of the new survey results from a combination of its intrinsically better sensitivity-per-unit-area and from the data analysis techniques utilised. The newly discovered emission accounts for approximately three-quarters of the total area of emission, yet contributes only ∼30% of the total integrated emission.

The map shows the Ring roughly subdivides into three main components: B223 to the south, B30 to the west, and an extended complex of low-level emission containing the clouds B35 and L1598/1599 to the north-east. These denser areas are the remains of density enhancements in the original GMC rather than material swept up by the expansion of the HII region.

2·1 Velocity Structure

Figure 2 shows that the Ring is split into two dominant velocity components. The southern complex lies around −2 km s^{-1}, while the other strong emission is at around 8 km s^{-1}. It is difficult to determine if weak emission spatially links the two, as we might expect from a continuous shell or ring structure. It seems unlikely that such a definite bifurcation in velocity could result entirely from the expansion of the HII region. More credible is the idea that we are dealing with the disruption of what was initially two distinct cloud complexes, with different initial velocities. Indeed, the southern part of the Ring appears spatially and kinematically connected to Barnard's Loop and its associated HI features (Zhang and Green 1991).

2.2 Clumps

The datacube was subdivided into individual emission features ('clumps'), using the CLUMPFIND algorithm (Williams, de Geus & Blitz 1994). We found 130 distinct clumps. The clump parameters are available in tabulated form that can be obtained via email from the authors.

3 Interpretation

3.1 Total Mass

We can make a direct estimate of the total molecular mass of the Ring via the relation $M_{\rm CO} \propto X d^2 S_{\rm CO}$, where d is the distance and $S_{\rm CO}$ is $W_{\rm CO}$ summed

 1323-3580/98/010070$05.00

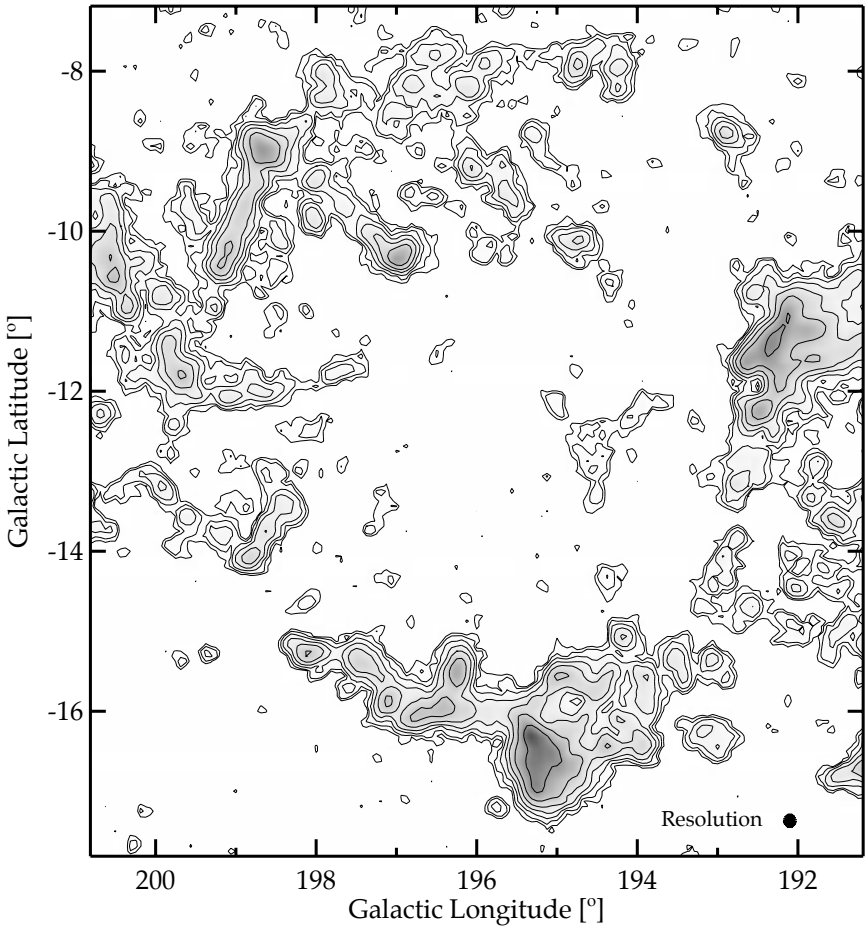

Figure 1—Zeroth moment map of velocity-integrated emission, $W_{\rm CO}$. Contours are at $0{\cdot}3$, $0{\cdot}6$, $1{\cdot}2$, $2{\cdot}4, \cdots$ K km s^{-1}. Emission covers the velocity range $[-10, +20]$ km s^{-1} with respect to the LSR.

over the angular extent of the cloud. Here X is the standard conversion factor $N_{\rm H_2}/W_{\rm CO}$, and we use the value of $X = (1{\cdot}06{\pm}0{\cdot}14){\times}10^{20}$ cm^{-2}(K km s^{-1})$^{-1}$ derived for the Orion region by Digel, Hunter & Mukherjee (1995). This is considerably lower than the $2{\cdot}6{\times}10^{20}$ cm^{-2}(K km s^{-1})$^{-1}$ used by MM. Therefore, even though we have detected a substantial amount more CO emission than MM, our mass estimate is slightly lower at $1{\cdot}1{\times}10^4$ M$_\odot$.

3·2 Kinematics

We consider a simple expanding shell model to fit to the clump peaks. Using code originally designed to model circumstellar masers (Yates & Cohen 1994), we obtain a reasonably good numerical fit to a model in which the shell expands at $\sim$16·5 km s^{-1} from datacube position $(v, l, b) = (3{\cdot}8, 195{\cdot}8, -12{\cdot}1)$, giving a present day radius of 30 pc and an expansion age of 1·8 Myr, younger than the 2–3 Myr derived by MM. This model shell closely follows the IRAS dust ring, unlike the MM shell, which is strongly emission biased towards their western clouds MM 2, 3, 6 and 7, which may not be involved in the HII region expansion.

The assumption of spherical expansion is far from adequate, however, and these preliminary results should be treated with caution. Velocity maps suggest that we are dealing with two flattened cloud complexes. Further work must be undertaken using expanding ring models, for example. We must also be careful which clumps to include in model fits. Only those directly interacting with the HII region should be used. IRAS and Hα images can help determine which parts of the region fall into this category. Diffuse Hα images (Isobe 1973; Gaustad 1997) clearly show that the southern B223 complex, in contrast to the rest of the Ring, has its optical bright rims facing *away* from the OB association. The bulk of the cloud is slightly in front of the HII region, and care should be taken in drawing conclusions from its kinematics, which could well be dominated by other influences, the expansion of the Ori-Eri Bubble for example.

4 Distribution of Young Stars

The distribution of low- to intermediate-mass young stars can be traced by excess Hα emission, which is a characteristic of T Tauri stars. We plot the

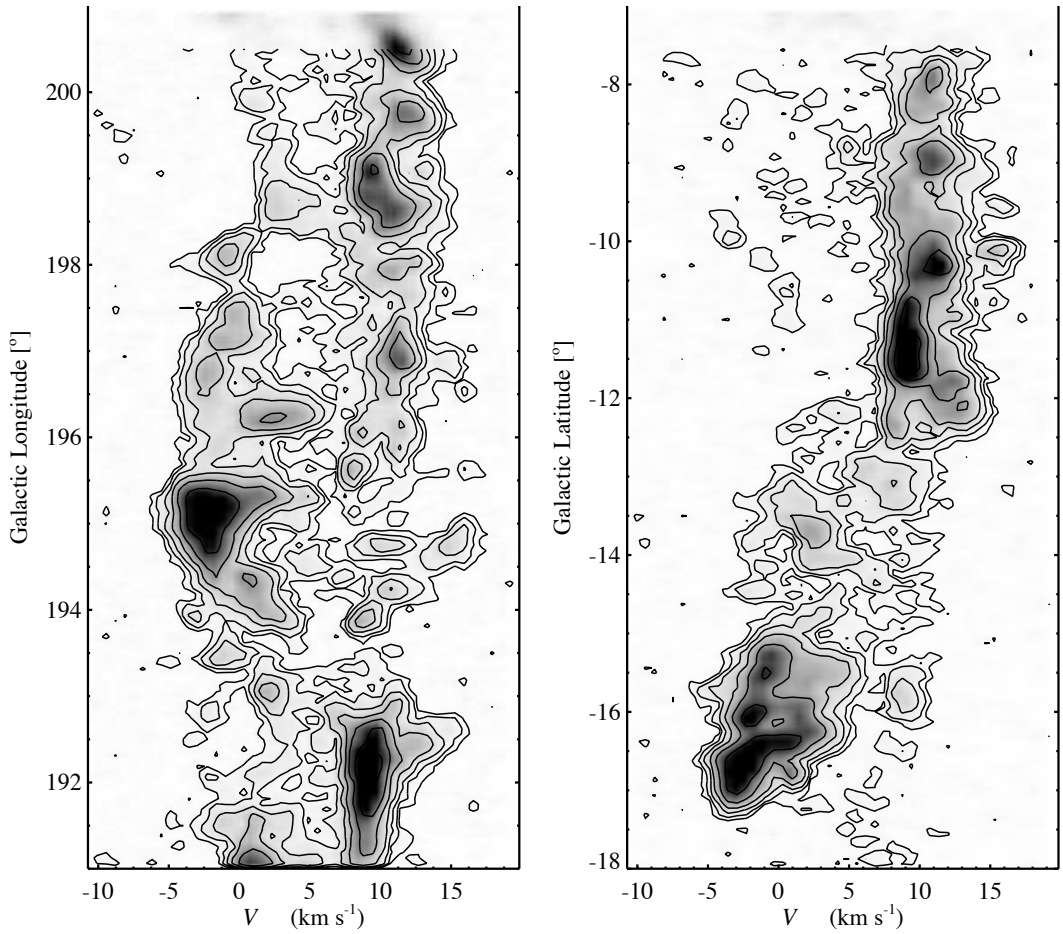

Figure 2—Velocity–position moment maps, (v, l) and (v, b). Contours are 0·12, 0·24, 0·48, 0·96, ... K.

catalogue members from the Hα point source survey of Duerr, Imhoff & Lada (1982) along with the OB stars in Figure 3.

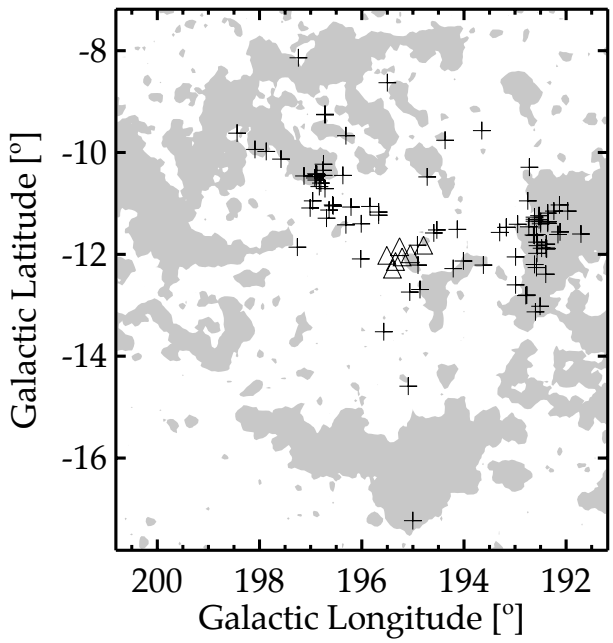

Figure 3—Hα-emitting stars (crosses) and OB stars (triangles) in the λ-Ori region.

This recent (<3 Myr) star formation has occurred almost exclusively in a thin band running though the northern part of the Ring, between the B35 and B30 complexes. This presumably traces the position of the 'fossil molecular cloud' (Duerr, Imhoff & Lada 1982), prior to disruption by the HII region. The position of the star formation band is roughly coincident with HI (Hartmann 1995) and diffuse Hα filaments. Given the identification of these filaments with the Orion-Eridanus Bubble (Brown, Hartmann & Button 1995), this is evidence for star formation triggered by some event causing compression of the primordial λ-Ori GMC along its southern edge.

5 Conclusions

- The results of this survey greatly improve on those of the older 1·2 m CO survey (MM). The lowest contour of our maps is around ten times lower than that of the MM survey.
- The spherically symmetric, single cloud model of HII region/cloud interaction is inappropriate here, despite the apparent symmetry of the region. We require a multi-cloud model which explains the two-component velocity structure.

- The CO correlates very well with IRAS 100μ except in several small regions of excess UV radiation: around the central OB cluster and the HII region S263 embedded within the B223 complex.
- A further worthy comparison is with Hα emission, particularly when considering the direct interaction between dense clouds and the stellar UV fields in the form of 'bright rims'. Hα images also enable us to determine which molecular clouds are associated with the HII region.

Acknowledgments

We thank Patrick Thaddeus, Tom Dame, Dap Hartmann, Sam Palmer and the rest of the mm-wave group at the CfA.

Brown, A. G. A., Hartmann., D., & Burton, W. B. 1995, A&A 300, 903
Digel, S. W., Hunter, S. D., & Mukherjee, R. 1995, ApJ, 441, 270
Digel, S. W., Lyder, D. A., Philbrick, A. J., Puche, D., & Thaddeus, P. 1996, ApJ, 458, 561
Duerr, R., Imhoff, C. L., & Lada, C. J. 1982, ApJ, 261, 135
Gaustad, J. E. 1997, Personal communication
Hartmann, D. 1995, Personal communication
Isobe, S. 1973, in Interstellar Dust and Related Topics, IAU Symposium 52, ed. J. H. Greenburg & H. C. van de Hulst (Reidel: Dordrecht), p. 433
Maddalena, R. J., & Morris, M. 1987, ApJ, 323, 179
Murdin, P., & Penston, M. V. 1977, MNRAS, 181, 657
Reich, W. 1978, A&A, 64, 407
Wade, C. M. 1957, PhD Thesis, Harvard University
Williams, J. P., de Geus, E. J., & Blitz, L. 1994, ApJ, 428, 693
Yates, J. A., & Cohen, R. J. 1994, MNRAS, 270, 958
Zhang, C. Y., & Green, D. A. 1991, AJ, 101, 1006
Zhang, C. Y., Laureijs, R. J., Chlewicki, G., Clark, F. O., & Wesselius, P. 1989, A&A 218, 231